Ab Initio Study of an $H_{24}O_{12}$ Zwitterion

David J. Anick

Harvard Medical School, McLean Hospital, Bowditch Building, 115 Mill St., Belmont, Massachusetts 02478

Received: September 30, 2002; In Final Form: December 19, 2002

An $H_{24}O_{12}$ zwitterionic water cluster based on the 4^45^4 cage geometry is described and studied at the B3LYP/6-311++G** level. The cluster's PES has two zwitterionic local minima, which are connected by low barrier pathways involving transfers of two protons, denoted H82 and H5U, along hydrogen bonds. The two zwitterionic minima sit in a broad megabasin that also contains two shallow saddles and a hilltop. All features lie within 0.5 kcal/mol of each other. The zwitterion converts to neutralized $(H_2O)_{12}$ clusters via proton transfers along any of eight embedded water wires. Optimized geometries for transition states and products for these neutralization reactions are computed. These neutralization pathways are endothermic at 77 K, suggesting that the zwitterion could be detected in a low temperature experimental system. Activation energies for neutralization range from 2.9 to 3.8 kcal/mol at 77 K and from 2.3 to 3.1 kcal/mol at 25 °C. Computed IR spectra for the zwitterion and its neutralized geometries are compared. The IR spectrum of the zwitterion has several modes involving coordinated vibration of H82 and H5U, which are not present in the spectra of the neutralized clusters. Benchmark comparisons against MP2/aug-cc-pVTZ show that B3LYP/6-311++G** may be superior to MP2/6-311++G** for proton transfer studies in water clusters.

1. Introduction

Water zwitterions, i.e., $H_{2n}O_n$ clusters in which the covalent bonding pattern is $(H_3O^+)(H_2O)_{n-2}(OH^-)$, are model systems in which coordinated transfers of multiple protons along water wires play a key role. Water wires figure importantly in a variety of chemical and biological processes.[1−6] The study of water zwitterions began with Stillinger and David [7] in 1980. They used a polarization model to study the $H_{16}O_8$ diamond zwitterion, in which the H_3O^+ and the OH^- are three H-bonds apart, and concluded that the zwitterion was probably unstable.

The first zwitterionic local minimum verified by ab initio methods was the $H_{10}O_5$ diamond studied by Lee et al.[8] and Tozer et al.[9] For the "reaction" consisting of coordinated transfer of the two water wire protons, they located stationary states for the zwitterion (reactant), transition state, and neutralized cluster (product). The electronic activation barrier, computed as the t-state electronic energy minus zwitterion electronic energy, was below 0.1 kcal/mol. This barrier became negative when ZPVE effects were added in, i.e., $\Delta G^{act} < 0$, suggesting that the $H_{10}O_5$ would not be isolable. Jensen et al.[10] subsequently reexamined the $H_{10}O_5$ zwitterion using the models HF/6-311++G**, MP2/6-311++G**, and MP4//MP2 and noted two exceptionally strong lines in its predicted IR spectrum near 2700 cm^{-1}.

Plummer[11] discovered a cube-based $H_{16}O_8$ zwitterion as part of her investigations of ionic defects in ice but did not analyze it in detail. Smith et al.[12] revisited two forms of the Stillinger−David diamond in 1999, studying it via B3LYP and MP2. They demonstrated that both Stillinger and David's "staggered" diamond and a second "eclipsed" form have zwitterionic PES local minima, which, like the Lee−Tozer−Jensen diamond, become unstable when ZPVE corrections are added in. The author similarly studied the cube zwitterion and a pentagonal prism ($H_{20}O_{10}$) zwitterion.[13] These also follow the pattern of being PES local minima with $\Delta G^{act} < 0$.

The $H_{24}O_{12}$ zwitterion that is the subject of this article uses the 4^45^4 H-bonding pattern found in Tsai and Jordan's "Cage 1" and "Cage 2" geometries (Figure 3 of ref 14), so we call it simply the "cage zwitterion". The bonding pattern of the cage is illustrated as Figure 1a. A plane projection of Tsai and Jordan's Cage 2 optimized at the B3LYP/6-311++G** level is shown in Figure 1b as an example of a low energy cage-based water cluster. The cage zwitterion was initially expected to be similar to the $H_{16}O_8$ diamond, the cube, and the pentagonal prism, but it turned out to have several features not seen in any previously reported zwitterion. These features include: (1) H-bonds adjacent to each ion with low barrier transfers, making it better described as $(H_5O_2^+)(H_2O)_8(H_3O_2^-)$ than as $(H_3O^+)(H_2O)_{10}(OH^-)$; (2) a broad megabasin containing two local minima, two saddle points, and a hilltop; (3) $\Delta G^{act} > 0$ for all eight water wire pathways; and (4) because the neutralized geometries are strongly polarized high-energy $(H_2O)_{12}$ clusters, the neutralization reactions are actually slightly endothermic at 77 K ($\Delta G^{neu} > 0$).

The model B3LYP/6-311++G** was used for most calculations. This model has undergone extensive validation for water cluster studies, via benchmark comparisons against MP2 results, most typically against MP2/6-311++G**.[12,13,15−18] However, comparisons of B3LYP/6-311++G** against very high accuracy methods such as MP2/aug-cc-pVTZ, specifically for proton transfer studies, are scarce. Benchmarking was therefore carried out for five model systems that were deemed representative of the calculations most relevant to the cage zwitterion. B3LYP/6-311++G** was compared with MP2/6-311++G** and with MP2/aug-cc-pVTZ. In four of five model systems B3LYP fared substantially better than MP2/6-311++G**, and in the fifth their deviations from MP2/aug-cc-pVTZ were similar. Based on these findings, B3LYP results are reported and used without MP2 corrections.

2. Description of the Cage Zwitterion

Figure 2a shows a plane projection of the B3LYP-optimzied cage zwitterion. The twelve oxygen atoms are labeled O1, ...,

10.1021/jp027098j CCC: $25.00
Published on Web 02/11/2003

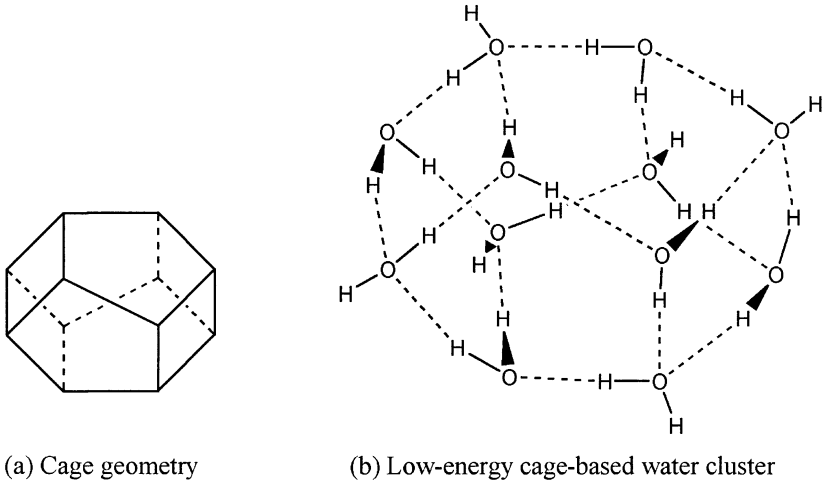

(a) Cage geometry (b) Low-energy cage-based water cluster

Figure 1. Illustrations of the $H_{24}O_{12}$ cage geometry.

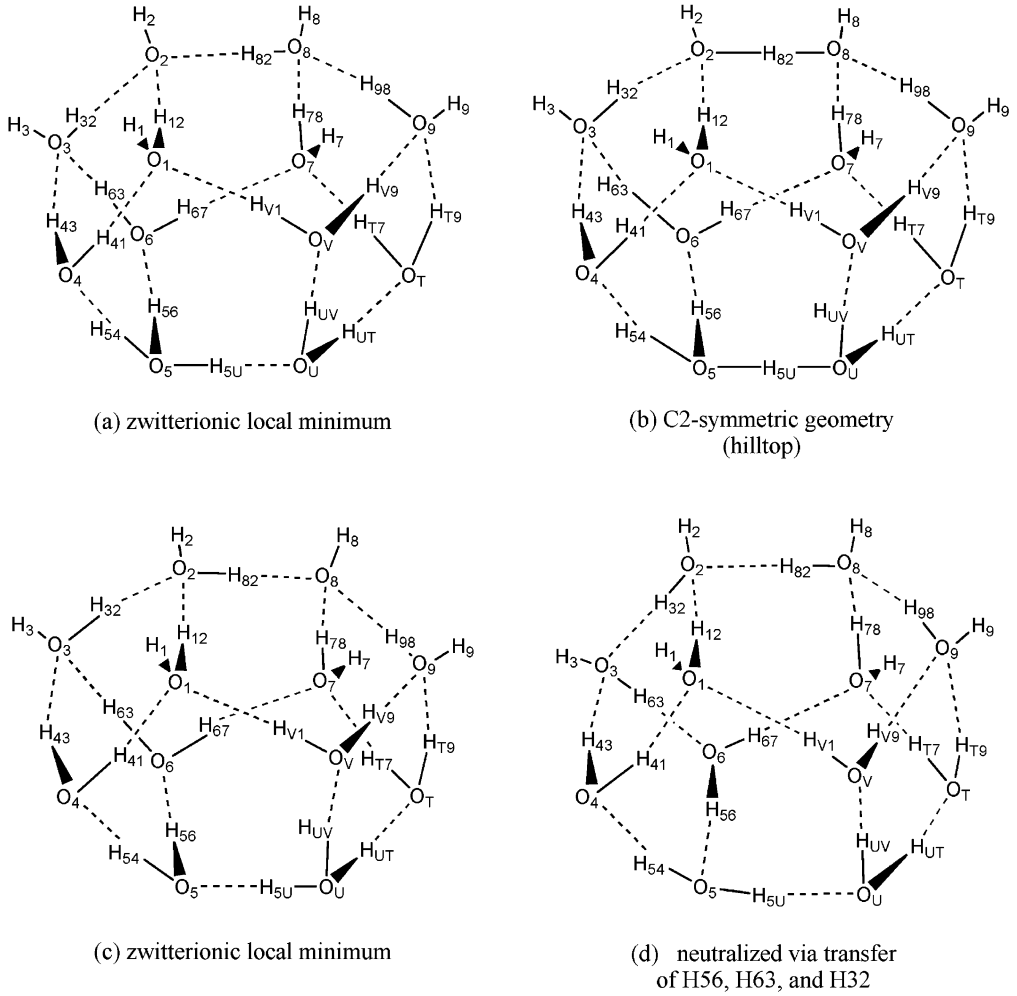

(a) zwitterionic local minimum (b) C2-symmetric geometry (hilltop)

(c) zwitterionic local minimum (d) neutralized via transfer of H56, H63, and H32

Figure 2. Stationary states related to the cage zwitterion.

O9, OT, OU, OV; think of T, U, V as the "digits" 10, 11, 12. Pendent (i.e., non-H-bonding) H's are labeled with a single digit derived from the O to which they are covalently bonded. Bonding H's are given two-digit designations for the two oxygen atoms that they join, with the O that is the donor in Figure 2a being listed first. In Figure 2a the H_3O^+ is at O5 and the OH^- is at O2.

Figure 2a "almost" has C_2 symmetry. If protons H82 and H5U are nudged into the centers of their H-bonds, and the cluster is reoptimized, the result is Figure 2b, which has C_2 symmetry around a vertical axis that passes through H82 and H5U. By rotating Figure 2a 180° around this axis, a second zwitterionic PES local minimum is obtained, shown as Figure 2c, which has its H_3O^+ at OU and its OH^- at O8.

Eight water wires, i.e., homodromic sequences of H-bonds, connect O5 and O2 in Figure 2a. The wires share some H-bonds and range in length from 3 to 5 H-bonds. The collection of water wires reflects an underlying structure that is best revealed by identifying four sets of oxygen atoms representing "strata" within the cage. The sets are $\mathscr{A}$ = {O5,OU}, $\mathscr{B}$ = {O4,O6,-

OT,OV}, $\mathscr{C}$ = {O1,O3,O7,O9}, and $\mathscr{D}$ = {O2,O8}. Figure 2a is positioned so that the sets appear as distinct horizontal bands. The oxygens in $\mathscr{C}$ and $\mathscr{D}$ carry pendent H's and the oxygens in $\mathscr{A}$ and $\mathscr{B}$ do not. Note that the O's in the set $\mathscr{A}$ are bonded only to each other and to the O's in $\mathscr{B}$; O's in $\mathscr{B}$ connect only to $\mathscr{A}$ and to $\mathscr{C}$; O's in $\mathscr{C}$ bond only to $\mathscr{B}$ and to $\mathscr{D}$; and O's in $\mathscr{D}$ connect only to $\mathscr{C}$ and to each other.

Each water wire contains one H-bond from $\mathscr{A}$ to $\mathscr{B}$, one from $\mathscr{B}$ to $\mathscr{C}$, and one from $\mathscr{C}$ to $\mathscr{D}$. Some also include a transfer within $\mathscr{A}$, within $\mathscr{D}$, or both. There are eight H-bonds that connect an O from $\mathscr{B}$ to an O from $\mathscr{C}$. Each of these H-bonds occurs in one and only one of the water wires, so water wires can be specified by their "$\mathscr{B}$-to-$\mathscr{C}$" bond and vice versa. For example, the proton H63 is in a $\mathscr{B}$-to-$\mathscr{C}$ bond and the unique water wire that uses it is O5−H56- - -O6−H63- - -O3−H32- - -O2. The neutral $(H_2O)_{12}$ cluster that results from transfer along this pathway is illustrated as Figure 2d.

The PES for the cage zwitterion has C_2 symmetry: each geometry other than Figure 2b has a "counterpart" geometry that is equivalent to it. For example, Figures 2a and 2c are both PES local minima and have identical electronic energies and bond lengths. The nontrivial "symmetry operation" can be described as increasing or decreasing each label by 6. For example, whatever is true of O5 in one geometry will be true of OU in its counterpart (5 + 6 = 11 = U), and the bond length O6−H67 in any geometry will equal the bond length OV−HV1 in its counterpart (6 + 6 = 12 = V, 7 − 6 = 1). Each of the eight water wires that start at Figure 2a has a counterpart that connects Figure 2c to a neutralized geometry. It follows that wires whose $\mathscr{B}$-to-$\mathscr{C}$ bonds are counterparts (e.g., the wire using H63 and the wire using HV9) will be completely equivalent, if one makes allowance for transfers of H5U and H82. Equivalent wires will have identical transition states and the same ΔG^{act} and the same ΔG^{neu}. Consequently, it is necessary to study only four different neutralization pathways, one from each equivalent pair. The set of four chosen in this article are the wires using H41, H43, H63, and HV1.

3. Methods

Nonbenchmark B3LYP geometry optimizations were carried out by Jaguar.[19] Jaguar's nonpseudospectral method was used throughout (keyword nops=1). Convergence criteria were tightened for transition states and for the points of the PES lying 0.5 kcal/mol or less above the minimum of Figure 2a (keywords gconv2=0.0001, gconv7 =0.00001). For PES points lying outside this contour, default convergence criteria were used. All benchmark calculations, all MP2 calculations, and all ZPVE/frequencies calculations were done by the GAUSSIAN98 suite of programs.[20]

All potential energy surface calculations shown are relaxed and not "vertical" scans, i.e., all parameters other than the scan variable(s) were fully optimized. For the benchmark PESs (Figures 3 and 4), steps of 2 pm changes in the r_{OH} distance were made, starting at r_{OH} = 100 pm. For the two-dimensional PES, steps of 4 pm or smaller were used starting at r_{OH} = 92 pm, and sampling steps were reduced to 3 pm or smaller within the 1 kcal/mol contour of Figure 5b. For both the benchmarks and the 2-D PES, energies are plotted as functions of symmetrized coordinates,[21−22] defined as R(HAB) = [d(OA−HAB) − d(HAB−OB)]/2 for the H-bond OA−HAB- -OB. Symmetrized coordinates have the advantage of permitting us to use and display the intrinsic symmetry of some H-bonds. It should be kept in mind, however, that the energies plotted are not strictly speaking the optimum for a given symmetrized coordinate, since the (donor-O−H) distance is what is held fixed during the optimization, not the difference of the two distances.

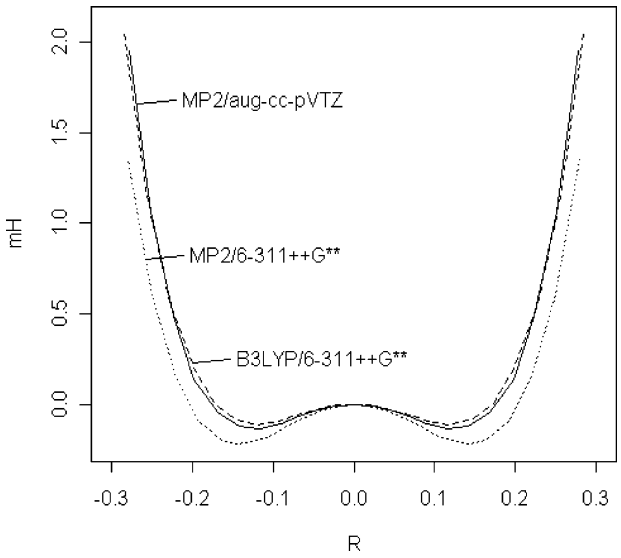

Figure 3. Benchmark: 1-D PES for $H_3O_2^-$ by three methods.

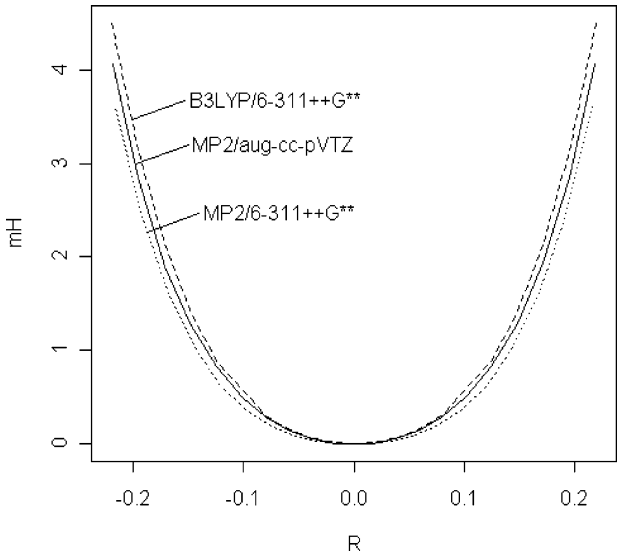

Figure 4. Benchmark: 1-D PES for $H_5O_2^+$ by three methods.

4. Benchmarks

4.1. Background. B3LYP/6-311++G** serves as a relatively fast method that gives reasonably accurate geometries of stationary states for small to medium size water clusters. However, past calculations have also indicated that B3LYP should be supplemented with MP2 level energy calculations. B3LYP/6-311++G** gives a value for the neutralization energy of the $H_{10}O_5$ diamond zwitterion that is more than 4 mH lower than Jensen and co-workers' MP2/6-311++G** value.[10] Christie and Jordan [23] found when comparing cationic pentamers ($H_{11}O_5^+$) that B3LYP energy differences could be off by as much as 1.7 kcal/mol as compared to MP2 results. In all of these, MP2//B3LYP energies are found to be much closer to MP2 than B3LYP. Pavese et al.,[24] computing a 2-D PES for $H_5O_2^+$, found that while B3LYP reproduced well the overall shape of the PES, some numerical values were significantly erroneous compared to an extremely accurate coupled cluster method.

4.2. Results. We undertook to assess how accurately B3LYP/6-311++G** could perform the type of calculations that were

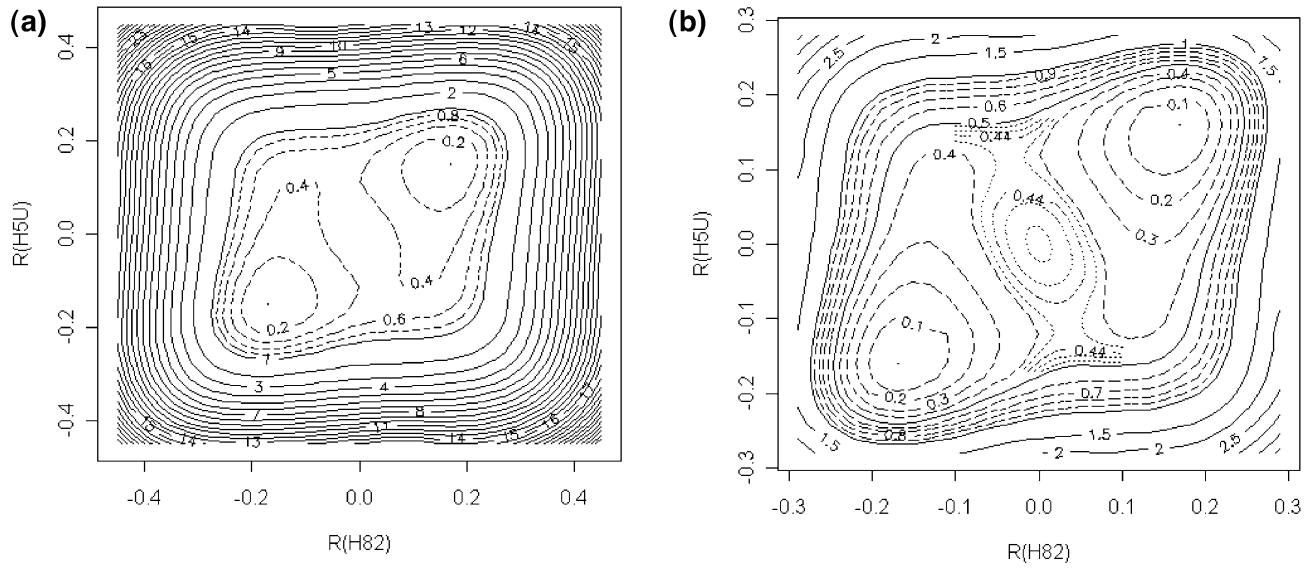

Figure 5. (a) Contour plot for 2-D PES (kcal/mol). (b) Contour plot for 2-D PES (kcal/mol), central region.

most relevant to the cage zwitterion. The 2-D PES computation for the cage zwitterion is similar to the computation of the 1-D PES for transfer of the bonding proton in the much simpler $H_5O_2^+$ and $H_3O_2^-$, systems. The 1-D PES for each of these was computed by B3LYP/6-311++G**, MP2/6-311++G**, and the presumably very accurate MP2/aug-cc-pVTZ. Three other model systems we considered were the $H_{10}O_5$ diamond, the H_8O_4 cyclic tetramer, and the $H_{16}O_8$ cube zwitterion. In each case, B3LYP and MP2/6-311++G** energies were compared against MP2/aug-cc-pVTZ, which was taken as the gold standard.

Results for the 1-D potential energy surfaces, plotted as functions of the symmetrized proton transfer coordinate, are shown as Figures 3 and 4. Figure 3 shows excellent agreement between B3LYP and MP2/aug-cc-pVTZ for the $H_3O_2^-$ system, with MP2/6-311++G** faring significantly worse. The minimum geometry as computed by both B3LYP and MP2/aug-cc-pVTZ has $r_{OH^*} = 112.0$ pm while MP2/6-311++G** places it at 109.5 pm. The height of the energy barrier between the minima is 0.12 mH by B3LYP, 0.21 mH by MP2/6-311++G**, and 0.13 mH by MP2/aug-cc-pVTZ, again favoring B3LYP.

The PES of $H_5O_2^+$ actually has two centrosymmetric local minima, one with C_s symmetry and one with slightly lower energy with C_2 symmetry that is the global minimum.[25−27] The two configurations differ via rotation of the non-H-bonding protons around the O−O axis. A 1-D relaxed PES scan can be computed by starting at either minimum and then decreasing r_{OH^*} in steps. The constrained minima obtained by starting from the Cs minimum retain C_s symmetry while those that start from the C2 minimum have C_1 symmetry. At some point, which occurs around $r_{OH^*} = 109$ pm for B3LYP, the Cs-symmetric constrained minima cease to be minima, i.e., the height of their barrier to rotation (with r_{OH^*} still fixed) becomes zero. The curves shown in Figure 4 were derived by starting with the global minimum and represent the C1 configurations only. For the $H_5O_2^+$ system, the error of B3LYP vs MP2/aug-cc-pVTZ is slightly greater than that of MP2/6-311++G** vs MP2/aug-cc-pVTZ, but of comparable magnitude.

As a benchmark for the computation of the electronic energy of neutralization, ΔE^{neu}, Jensen and co-workers' calculations for $H_{10}O_5$ were extended to include MP2/aug-cc-pVTZ. The t-state for the $H_{10}O_5$ diamond is very close to the zwitterion, so $H_{10}O_5$ was not considered to be a representative system for benchmarking the electronic energy of activation, ΔE^{act}. In the cage zwitterion, the t-states have very different geometries from the zwitterionic minima. The system used instead is the S4-symmetric cyclic H_8O_4 tetramer, which contains a cyclic water wire of length 4.[28−30] The t-state for transfer along this water wire has all four protons moved to the midpoints of their H-bonds, a structure with D_{2d} symmetry.[15]

Table 1 shows the results. The $H_{10}O_5$ structures were evaluated by MP2/aug-cc-pVTZ//B3LYP but were not optimized at the higher level, due to the computational demand. The above-mentioned gap of 4 mH between the B3LYP and MP2 calculations for ΔE^{neu} nearly disappears when the larger basis set is used: compared to MP2/aug-cc-pVTZ//B3LYP, B3LYP's error is less than one tenth of the error of MP2/6-311++G**. Similarly, B3LYP substantially outperformed MP2/6-311++G** when it came to ΔE^{act} for the tetramer. While one can question whether MP2//B3LYP provides an adequate benchmark, the seven comparisons in Table 1 where a full MP2 optimization was done support the premise that the difference between MP2 and MP2//B3LYP is minor or insignificant for these systems. Because these results, which strongly favor B3LYP, were not as expected, a final benchmark was carried out comparing the three methods' predictions for both ΔE^{act} and ΔE^{neu} for the cube zwitterion. The results, also listed in Table 1, again dramatically support the superiority of B3LYP over MP2/6-311++G**.

4.3. Discussion. With the exception of the 1-D PES for $H_5O_2^+$, where the methods' errors were about equal, B3LYP/6-311++G** consistently outperformed MP2/6-311++G**. B3LYP appeared especially well suited for computing energy differences among stationary states. On this basis, B3LYP without MP2 correction was used for all calculations on the cage zwitterion.

Caution should be exercised in generalizing this finding. These benchmarks only compared structures that differ solely by transfers of one or more protons. Note that this description does not apply to Christie and Jordan's comparisons[23] of local minima having distinct connectivity patterns, where B3LYP fared somewhat worse than MP2/6-311++G**. Christie and Jordan also noted that B3LYP's worst failures came when comparing structures with different numbers of H-bonds. Pavese and co-workers' findings of significant error for B3LYP when computing some features of the 2-D PES of $H_5O_2^+$ should also be remembered, though it is of interest that our calculations

TABLE 1: Benchmark Comparisons of Electronic Energies of Stationary States Related by Proton Transfers (a.u.)

system and geometry	B3LYP/ 6-311++G**	MP2/ 6-311++G** // B3LYP	MP2/ 6-311++G**	MP2/ aug-cc-pVTZ // B3LYP	MP2/ aug-cc-pVTZ
$H_3O_2^-$ min	−152.3328182	−151.9600382	−151.9601855	−152.0744921	−152.0745811
$H_3O_2^-$ t-state (C_2 symmetry)	−152.3327031	−151.9598261	−151.9599693	−152.0743602	−152.0744502
ΔE^{act} (mH)	**0.1151**	0.2121	**0.2162**	0.1319	**0.1309**
H_8O_4 min (S_4 symmetry)	−305.8831880	−305.1491025	−305.1495859	−305.3613560	−305.3615352
H_8O_4 t-state (D_{2d} symmetry)	−305.8467860	−305.1076526	−305.1079372	−305.3251070	−305.3255008
ΔE^{act} (mH)	**36.4020**	41.4499	**41.6487**	36.2490	**36.0344**
$H_{10}O_5$ diamond zwitterion (C_3 symmetry)	−382.3243975	−381.4040444	−381.4046068[a]	−381.6746624	
$H_{10}O_5$ diamond neutralized	−382.3528069	−381.4365466	−381.4371815[a]	−381.7028111	
ΔE^{neu} (mH)	**−28.4094**	−32.5022	**−32.5747**	**−28.1487**	
$H_{16}O_8$ cube zwitterion (C_{3v})	−611.7663535	−610.2980078	−610.2989427	−610.7273609	
$H_{16}O_8$ cube t-state	−611.7621534	−610.2941979	−610.2951696	−610.7231401	
ΔE^{act} (mH)	**4.2001**	3.8099	**3.7731**	**4.2208**	
$H_{16}O_8$ cube neutralized	−611.7798390	−610.3153729	−610.3162062	−610.7407370	
ΔE^{neu} (mH)	**−13.4855**	−17.3651	**−17.2635**	**−13.3761**	

[a]These data were also reported in ref 10.

suggest that $H_5O_2^+$ may be anomalously "bad" for B3LYP. A further mitigating factor is that the basis sets used by Pavese et al. did not include diffuse functions, and the inclusion of diffuse basis functions can dramatically improve the reliability of both MP2 and B3LYP for water cluster computations.

Table 1 suggests that the problem with MP2/6-311++G** is that the basis set is too small, whereas the same basis set appears adequate for B3LYP. This is consistent with other observations regarding B3LYP and MP2.[31−32] Working with organic molecules, Stephens et al.[31] noted that B3LYP "saturates" more quickly than MP2 in the sense that the Kohn−Sham limit is well approximated with a smaller basis set. For this reason they recommended that B3LYP be used with 6-31G*, though for water cluster studies a triple-ζ quality basis with polarization and diffuse functions is necessary in order to obtain accurate geometries.

5. Potential Energy Surface

5.1. Background. The importance of the Zundel complex $H_5O_2^+$ and its anionic counterpart $H_3O_2^-$, for the understanding of proton transfer in aqueous systems, can hardly be overstated. Both complexes have been studied extensively from ab initio,[22,33−39] molecular dynamics,[21,40−46] and experimental perspectives,[47−51] and this article cannot do justice to the huge literature on them. The occurrence of an embedded $H_5O_2^+$ and an embedded $H_3O_2^-$ make this literature relevant to the cage zwitterion, and a few basics are recounted next.

The PES of $H_5O_2^+$ has a centrosymmetric minimum and a wide nearly flat central region, as illustrated in Figure 4. At the global minimum (C_2 symmetry) the O−O separation is about 241 pm. As the O−O distance increases, the potential shifts to double well, and the barrier height grows as the oxygens continue to separate.[22,24] The anharmonicity of the potential makes it difficult to estimate the ZPVE contribution due to vibrational modes of the O- -H*- -O component. Using 2D, 3D, and 4D adiabatic potentials, Vener et al.[34,35] found that the harmonic approximation yields the correct IR spectrum at a low temperature (1 K) but not at a high kinetic temperature (360 K).

The PES of $H_3O_2^-$ has a double well potential, as illustrated in Figure 3. The O−O separation at the global minimum is 247 pm, and at the C_2 symmetric t-state between minima it is 244 pm. Molecular dynamics simulations show that the bonding proton H* in $H_3O_2^-$ freely crosses the barrier but spends most of its time being associated with one O or the other.[21] Like $H_5O_2^+$, as the O−O separation increases the barrier height rises, eventually replacing the situation of a delocalized bonding proton H* with one that forces H* to choose a covalent bond with one O or the other. The transition occurs when the barrier height falls in the range of 2 to 4 kcal/mol.[21,52]

While $H_5O_2^+$ and $H_3O_2^-$ have each been studied extensively, the author is not aware of any previous attempt to study a water cluster that contains them both. One of the interesting questions posed by the cage zwitterion is how the proximity of the $H_5O_2^+$ might alter the behavior of the $H_3O_2^-$ and vice versa. If there were very little interaction, as well as little influence from the "$\mathcal{B}$" and "$\mathcal{C}$" level H_2O's, the 2-D relaxed PES might look like $F(x,y) = f(x) + g(y)$, where f is the function in Figure 3 and g is the function in Figure 4. This function would have two minima, both of them having H5U (the bonding proton of the $H_5O_2^+$ component) at the center of its H-bond, with a single saddle of height 0.12 mH between them. The PES does not look like this, so there are clearly some significant interaction terms. Another reason to study the PES is to assess the extent of anharmonicity at the zwitterionic minima. Anharmonicity could have a significant effect on the cluster's ZPVE and hence on its total free energy and stability.

5.2. Results. Figures 5a and 5b show the relaxed or adiabatic 2-D PES for the cage zwitterion. The x-axis is the symmetrized coordinate for O8- -H82- -O2, i.e., $R(\mathrm{H82}) = [d(\mathrm{H82-O2}) - d(\mathrm{O8-H82})]/2$, and the y-axis is the symmetrized coordinate for O5- -H5U- -OU, i.e., $R(\mathrm{H5U}) = [d(\mathrm{H5U-OU}) - d(\mathrm{O5-H5U})]/2$. For Figure 5a, solid contours are drawn at intervals of 1 kcal/mol, starting with "zero" being the energy of the minima, Figures 2a and 2c. Dashed contours are drawn 200 cal/mol apart for the region below 1 kcal/mol. Figure 5b focuses on the central region, with solid contours 0.5 kcal/mol apart, dashed contours at 100 cal/mol and, within a central rectangle, dotted contours showing changes of 20 cal/mol. The principal features of interest are the C_2 symmetry, the two minima, the two saddles, and the central hilltop. Energy rises quite steeply once $|R(\mathrm{H82})|$ or $|R(\mathrm{H5U})|$ exceeds 0.3 Å. At the central hilltop,

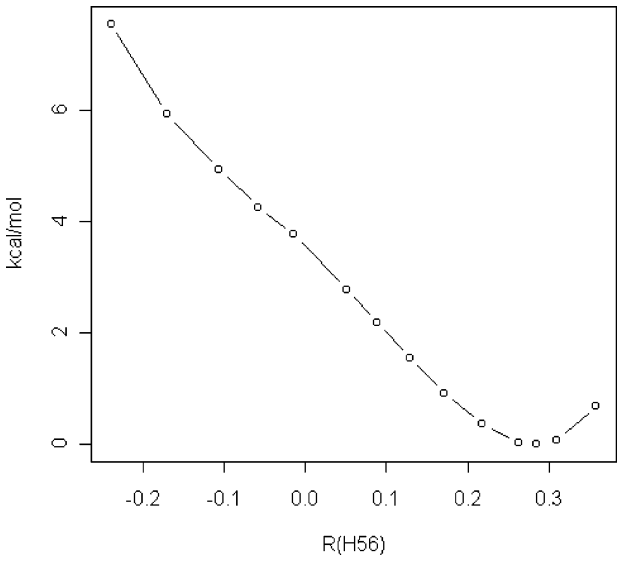

Figure 6. 1-D relaxed PES for transfer of H56.

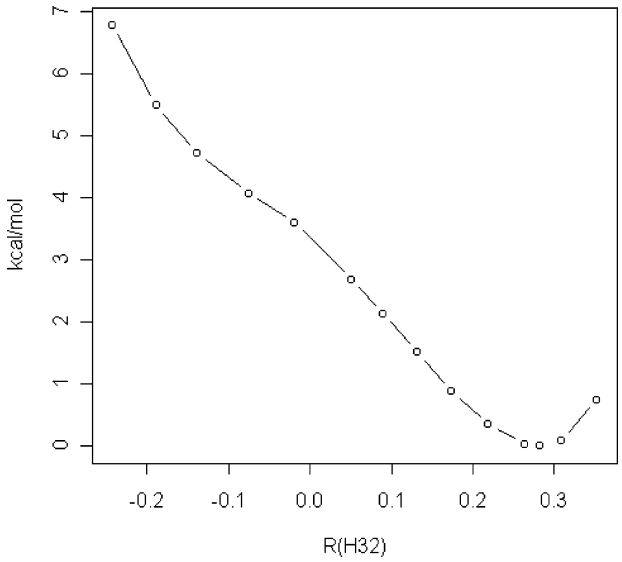

Figure 7. 1-D relaxed PES for transfer of H32.

d(O2−O8) = 2.422 and d(O5−OU) = 2.415. At either minimum these bond lengths are d(O2−O8) = 2.478 and d(O5−OU) = 2.460.

For much of the region within the 0.5 kcal/mol contour the PES is extremely flat. Early in the process of exploring the cage zwitterion, the Jaguar program indicated that sharpened convergence criteria for an unconstrained minimum had been met, at a point whose symmetrized coordinates are (−0.118, 0.084). This point lies on the wide "shelf" or "plateau" between the 0.3 and 0.4 kcal/mol contours. Subsequent calculations of the PES near this point with steps of 1 pm verified that despite the very small gradient there is no actual local minimum.

While we have focused on the PES for transfers of the two protons H82 and H5U, a reasonable question is what the PES looks like for transfers of other bonding protons in Figure 2a. Are there zwitterionic local minima with the H_3O^+ located somewhere other than O5 or OU, or with the OH^- located somewhere other than O2 or O8? Are there other low-barrier proton transfers? To explore these questions, we computed the 1-D PES in which a proton adjacent to the H_3O^+ or the OH^- was transferred by steps to its acceptor O while all other parameters were relaxed. Figure 6 shows the results for transfer of H56, with electronic energy plotted as a function of the symmetrized coordinate R(H56) = [d(O6−H56) − d(O5−H56)]/2. The range examined runs from d(O5−H56) = 0.97 Å to d(O6−H56) = 1.00 Å. Electronic energy increases monotonically as H56 is moved away from the position it has in the local minimum (Figure 2a), where R(H56) = 0.285 Å, and there is no local minimum with the H_3O^+ located at O6. The fact that the energy climbed by nearly 4 kcal/mol as H56 reached the midpoint of the O5−O6 H-bond showed that this transfer does not qualify as "low barrier". The same pattern was found for transfer of H54. Similarly, no local minima were found having the OH^- located anywhere in the $\mathcal{O}$ stratum. Results for transfer of H32 to O2 (thus moving the OH^- from O2 to O3), shown as Figure 7, were representative. Figure 7 plots electronic energy as a function of the symmetrized coordinate R(H32) = [d(O2−H32) − d(O3−H32)]/2.

5.3. Discussion. The shape of the 2-D PES confirms that significant interactions occur among $H_5O_2^+$, $H_3O_2^-$, and the other H_2O's. A partial qualitative explanation for the shape may be found in the fact that the O2−O8 and O5−OU axes are neither parallel nor perpendicular. At the hilltop geometry (Figure 2b) both are perpendicular to the symmetry axis H82−H5U, and the dihedral angle O2−H82−H5U−O5 equals 50.5°. If one compares, say, the point P1 = (0.1, 0.1) in the upper right quadrant (URQ) of Figure 5b with the point P2 = (−0.1,0.1) in the upper left quadrant (ULQ), H82 and H5U are further apart at P1 than they are at P2, so the electrostatic repulsion between them is greater at P2. Figure 8 illustrates how these distance relationships come about, with a view of the cage zwitterion from above. The URQ is the region of PES where H82 is closer to O8 than to O2 and H5U is closer to O5 than to OU; the ULQ is where H82 is closer to O2 than to O8 and H5U is closer to O5 than to OU; and likewise for the lower quadrants having H5U closer to OU. The H82−H5U repulsion energy is greater in the ULQ and lower right quadrant than at comparable points in the URQ and lower left quadrant, and this may help explain why the potential energy minima occur in the upper right and lower left quadrants while energy in the other quadrants is somewhat higher. This can also help to account for contours appearing to be "stretched" in the upper right−lower left direction.

An MD simulation of the cage zwitterion having enough accuracy to predict the long-term distribution of H82 and H5U is for now computationally infeasible. However, since the bonding protons in $H_5O_2^+$ and $H_3O_2^-$ can easily surmount barriers of 1 or 2 kcal/mol (depending on O−O distance), we extrapolate that H82 and H5U range freely within at least the 2 kcal/mol contour of Figure 5. This represents an exceptionally broad region of delocalization for a pair of protons in a neutral water cluster. In particular, it shows the protons' mobility is significantly greater than what it would be if the PES were equal to the harmonic (or local parabolic) approximation based at either of the minima of Figure 5. If V_{harm} denotes the potential obtained by extending the harmonic approximation at Figure 2a over the whole 2-D space, then the region where a hypothetical ground-state proton moving in the potential V_{harm} would have positive kinetic energy is an ellipse lying entirely within the URQ. Thus the harmonic approximation cannot be considered to be valid, at least for H82 and H5U. Clary and co-workers' concept of an "H-Density" for a water cluster[53] may ultimately be needed for an accurate description of the behavior of H82 and H5U.

The high degree of mobility for the protons H82 and H5U can be expected to cause a substantial lowering of the ZPVE for the cage zwitterion, compared with what the harmonic approximation at Figure 2a would predict. Mobility-based

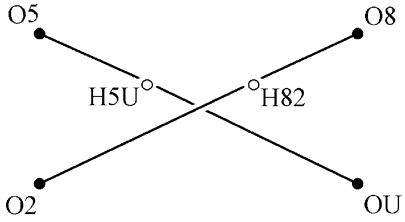

(a) Point P1, upper right quadrant
H82 nearer to O8, H5U nearer to O5

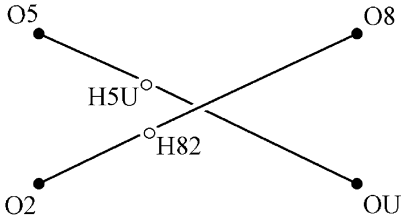

(b) Point P2, upper left quadrant
H82 nearer to O2, H5U nearer to O5

Figure 8. Relative positions of H_{82} and H_{5U} in two PES quadrants.

lowering of the ZPVE for the zwitterionic state, without similar lowering of the ZPVE for the neutralized geometries, has a bearing on the important question of the stability of the cage zwitterion. Although the extent of the effect cannot now be accurately predicted, its direction is to render the zwitterion more stable. The effect is like other "resonance" phenomena in quantum mechanics in which the occurrence of two (or more) minima separated by low barriers results in a ground state of lower energy than any one of the minima can support on its own.

6. Neutralization Pathways and Energies

6.1. Background. Neutralization of acid and base in aqueous solution is one of the fastest chemical reactions known, with a second-order rate constant of 1.4×10^{11} L mol^{-1} s^{-1}.[54] The Grötthaus mechanism[55] is widely accepted as an explanation for rapid proton mobility in water. Molecular dynamics simulations of transfers along isolated water wires containing an excess proton support the stepwise Grötthaus mechanism (with the modification that the excess proton spends much of the time being shared between two O's) and show that a transfer can be completed in less than a picosecond.[56−61] The equilibrium constant of $K_w = 10^{-14}$ corresponds to a free energy of neutralization of $\Delta G^{neu} = -21.4$ kcal/mol at 25 °C. Taken together, these facts paint a picture of $H_3O^+ - OH^-$ neutralization in bulk water as quick and irreversible, with the H_3O^+ and OH^- coming together via very fast single proton transfer steps.

This picture does not necessarily apply to neutralization of isolated gas-phase water zwitterions. One difference concerns pathways of neutralization. These have been studied for the $H_{10}O_5$ diamond, the $H_{16}O_{10}$ diamonds, the cube, and the length−three water wires of the pentagonal prism. In each case, a single transition state was identified. Neutralization occurs via coordinated movement of all three (or two in the case of $H_{10}O_5$) water wire protons. The t-states for neutralization of the cage zwitterion turn out to be most similar to those of the pentagonal prism, so we review briefly the prism t-state geometries.[13] All three length-three water wires follow the same pattern. If the wire is denoted OA−HAB- - -OB−HBC- - -OC−HCD- - -OD, with the H_3O^+ at OA and the OH^- at OD, then the zwitterion, t-state and neutralized geometry (product) are illustrated schematically in Figure 9. Figure 9 reproduces O−O distances to scale but O−H distance differences are exaggerated slightly for better clarity. At the prism's t-states, proton HAB has transferred, HBC has not transferred, and HCD is about in the middle of its H-bond.

A second difference from the bulk water picture lies in ΔG^{neu}. A range of neutralization energies has been found for zwitterions, ranging from −19.2 kcal/mol for $H_{10}O_5$ to −7.1 kcal/mol for one of the $H_{20}O_{10}$ prism pathways (these are B3LYP figures with ZPVE and thermal correction, cf. section 4). The cube and prism zwitterions are less polarized than their

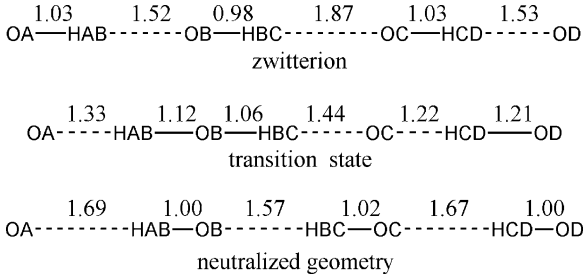

Figure 9. Water wire distances (Å) for $H_{20}O_{10}$ prism (ref 13).

corresponding neutralized geometries. There is an inverse correlation between $-\Delta G^{neu}$ and the neutralized cluster's dipole moment D^{neu}, with larger D^{neu} values corresponding to smaller values of $-\Delta G^{neu}$.

The $D^{neu}-\Delta G^{neu}$ connection was interpreted in ref 13 as follows. Referring to Figure 2d as an example of a neutralized cluster, note that the 12 constituent H_2O's nearly all have the *z*-component of their dipole moments pointing upward. The cluster as a whole inherits a large upward-pointing dipole moment. Zwitterion formation (Figure 2a) involves net movement of protons downward, from the positive toward the negative pole of the dipole, providing an electrostatic energy decrease that partially offsets the energetic cost of ion pair formation. The larger the cluster dipole moment D^{neu}, the larger the offset. There is a similar correlation between D^{neu} and the free energy of activation ΔG^{act}, with larger D^{neu} values correlating with larger ΔG^{act} values. One reason for studying the cage zwitterion was to see whether these trends would continue, and to see how small ΔG^{neu} and how large ΔG^{act} might become.

6.2. Results. As noted in section 2, the eight water wires connecting the H_3O^+ and the OH^- fall into four equivalent pairs and only one member of each pair needs to be studied. For the four selected wires, the neutralized cluster and t-state were optimized at the B3LYP/6-311++G** level. For the t-states, good initial guesses were obtained by performing constrained minimizations in which the distances HAB−OB and HCD−OD were fixed at 113 pm (cf. Figure 9) and Jaguar's convergence behavior was improved by lowering the trust radius from its default value of 0.1 to 0.04.

Table 2 lists, for each pathway, highlights of the three geometries. The t-states are similar to one another and conform to the pattern of Figure 9, with the modification that HCD has transferred fully to OD and no longer sits at or near the middle of the OC−OD bond. For the length 4 pathway O5−OU−OV−O1−O2, with $\mathscr{B}$-to-$\mathscr{C}$ proton HV1, the OA−HAB−OB distances differ from those of the other three pathways, which have length 3. The reason for the difference is that "OA" is O5, where the H_3O^+ is, for the length 3 pathways but "OA" is OU, one H-bond removed from the H_3O^+, for the HV1 pathway. Dipole moments are included in Table 3. Notice that, as with other zwitterions, D^{neu} significantly exceeds D^{ts} and D^{zw}.

TABLE 2: Highlights of Zwitterion, Transition State, and Neutralized Cluster Geometries (Å)

pathway	geom	OA−OB	OB−OC	OC−OD	OA−HAB	HAB−OB	OB−HBC	HBC−OC	OC−HCD	HCD−OD
O5−O4	zw	2.594	2.792	2.605	1.016	1.591	0.979	1.844	1.015	1.596
−O1−O2	ts	2.428	2.458	2.429	1.295	1.137	1.088	1.375	1.299	1.136
(H41)	neu	2.641	2.555	2.635	1.646	1.004	1.534	1.024	1.639	1.004
O5−O4	zw	2.594	2.824	2.591	1.016	1.591	0.977	1.898	1.018	1.581
−O3−O2	ts	2.427	2.459	2.436	1.297	1.136	1.085	1.381	1.327	1.116
(H43)	neu	2.638	2.555	2.625	1.647	1.003	1.534	1.025	1.630	1.004
O5−O6	zw	2.592	2.786	2.591	1.016	1.586	0.979	1.829	1.018	1.581
−O3−O2	ts	2.424	2.462	2.429	1.285	1.143	1.078	1.388	1.306	1.128
(H63)	neu	2.648	2.548	2.623	1.656	1.002	1.524	1.026	1.624	1.005
O5−OU−OV[a]	zw	2.704[a]	2.809	2.605	0.992[a]	1.726[a]	0.977	1.840	1.015	1.596
−O1−O2	ts	2.428	2.461	2.421	1.294	1.136	1.080	1.382	1.260	1.165
(HV1)	neu	2.649	2.549	2.630	1.653	1.002	1.524	1.025	1.629	1.005

[a] OA of water wire is OU, and H_3O^+ is at O5 (see text).

TABLE 3: Calculation of ΔG^{act} and ΔG^{neu} at 77 K and 25 °C for Each of Eight Pathways of Neutralization (kcal/mol; via B3LYP)

		B-to-C Proton of Neutralization Pathway			
		H_{41} or H_{T7}	H_{43} or H_{T9}	H_{63} or H_{V9}	H_{67} or H_{V1}
transition state	ΔE^{act}	10.359	10.234	9.541	9.809
	ZPVE correction	−4.661	−4.076	−4.625	−5.025
	thermal corr. at 77 K	−0.105	−0.113	−0.115	−0.091
	ΔG^{act} at 77 K	5.593	6.045	4.801	4.693
	thermal corr. at 25 °C	−1.157	−1.165	−1.232	−0.984
	ΔG^{act} at 25 °C	4.541	4.993	3.684	3.800
	dip M (Debye)[a]	12.34	11.97	12.10	12.51
neutralized geometry	ΔE^{neu}	1.094	1.405	0.540	0.015
	ZPVE correction	0.861	0.984	0.979	0.850
	thermal corr. at 77 K	−0.363	−0.368	−0.352	−0.349
	ΔG^{neu} at 77 K	1.592	2.021	1.167	0.516
	thermal corr. at 25 °C	−4.935	−4.879	−4.816	−4.858
	ΔG^{neu} at 25 °C	−2.980	−2.490	−3.297	−3.993
	dip M (Debye)[a]	15.55	15.40	15.47	15.53

[a] Dipole moment of the zwitterionic local minimum (Figure 2a) is 9.12 D.

Table 3 lists the contributions to the free energy of each geometry at 77and 298.15 K. Within each column of Table 3, "zero" is taken as the energy of the zwitterion (Figure 2a), as computed using the harmonic approximation. At 77 K, all neutralization pathways are endothermic, with ΔG^{neu} ranging from 0.32 to 1.27 kcal/mol; this energy range is 2.1 to 8.3 times k_BT, at 77 K. The range of ΔG^{act} values is 2.9 to 3.8 kcal/mol, or 19 to 25 times k_BT. At 25 °C these ranges are −2.6 k_BT to −4.2 k_BT for ΔG^{neu} and 3.9 k_BT to 5.3 k_BT for ΔG^{act}. Referring to the argument in section 5 that the harmonic calculation of ZPVE for the zwitterion probably gives a value that is too high, the true values of ΔG^{act} and ΔG^{neu} can be expected to be somewhat greater than the values listed in Table 3.

6.3. Discussion. The idea of neutralization being endothermic or close to isoenergetic for a water zwitterion may seem paradoxical at first. If twelve H_2O's in bulk water were to randomly arrange themselves into one of the neutralized cage geometries, such as Figure 2d, dissociation could readily occur within that cluster. This does not contradict the ΔG^{dissoc} of 21.4 kcal/mol, because such a cluster will very rarely form spontaneously. Compared to a low energy cage-based $(H_2O)_{12}$ like Figure 1b, the energy of Figure 2d is 13.4 kcal/mol higher (B3LYP+ZPVE+thermal correction to 25 °C), and there is the additional low likelihood, hard to estimate, of forming the cage at all.

Our results dovetail very nicely with the molecular dynamics simulations of autodissociation in water conducted by Geissler et al.[62] They proposed that rare fluctuations in local solvent electric fields facilitate the formation of ion pairs along water wires of length three to five. The ions may subsequently migrate further apart, especially if the wire "breaks" and becomes unavailable for reneutralization. Geissler and co-workers found that the combined effect of many solvating H_2O's was needed for stabilizing the separated ion pair. The cage zwitterion shows that eight solvating H_2O's (i.e., along with the four in the water wire) can be enough to make ion pair formation approximately isoenergetic. It also illustrates how Geissler and co-workers' "solvent electric field coordinate" arises from a local microcluster dipole moment due to many approximately aligned H_2O's.

Our data predict that the cage zwitterion might be detectable in an experimental system at 77 K. It would exist in equilibrium with the four neutralized geometries; but with ΔG^{neu} starting at 2.1 k_BT, the population of zwitterions would be at least four times greater than that of the lowest energy neutralized cluster (the ratio is 2 $\exp(-\Delta G^{neu}/k_BT)$ because each neutralized structure represents two geometries that are reached by distinct but equivalent pathways from the zwitterion). Observing a zwitterion will require that it not "melt", i.e., undergo rearrangements of its H-bonding pattern. For low-energy cube-based water clusters Pedulla and Jordan [63] estimated the melting temperature to be in the range 112 to 250 K, depending on the model used, while Rodriguez et al.[64] found the melting transition to occur at 160 K. These give us a ball park figure for the melting temperature of similar clusters, including $(H_2O)_{12}$ cages. However, the strong degree of polarization of our clusters could mean that they melt at a lower temperature.

If the cage zwitterion is detectable in a low-temperature system, we offer the following speculation on how it might be made. While accreting H_2O's to form small clusters, impose a constant electric field. With a strong enough field, a highly polarized cluster like Figure 2d, which can lower its energy substantially by aligning with the field, might be energetically

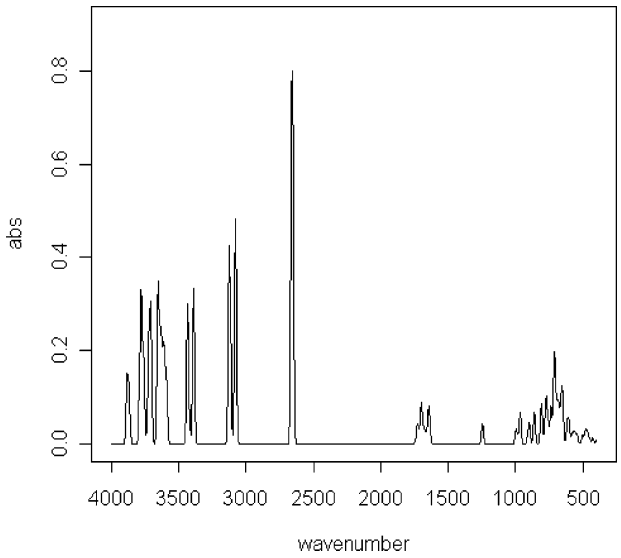

Figure 10. Computed IR spectrum for $(H_2O)_{12}$ of Figure 2d.

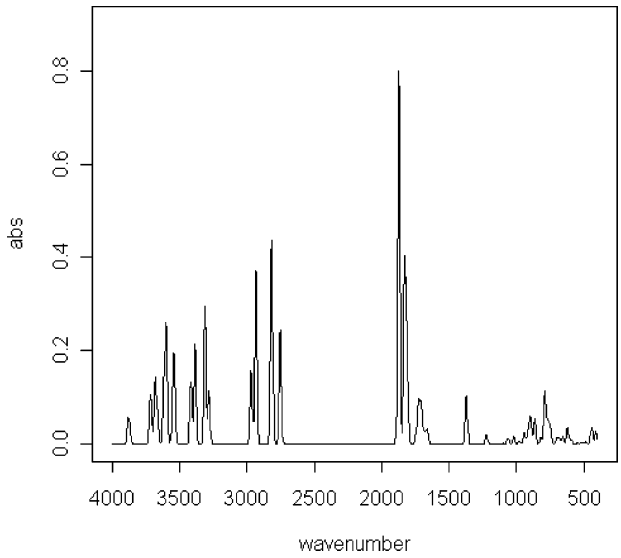

Figure 11. Computed IR spectrum for zwitterion (Figure 2a).

favored over less polarized ones such as Figure 1b. (We have already noted that Figure 1b is favored over Figure 2d in the absence of an external field.) If the electric field were subsequently turned off, the cluster could spontaneously convert to the zwitterion. This outline is speculation only: we have not yet conducted ab initio studies to verify that polarized clusters, let alone polarized cage-like clusters, are more likely to form in the presence of an electric field, nor can we suggest how strong the field would need to be.

7. Computed Infrared Spectra

7.1. Background. Vibrational spectra of water clusters is a huge and well-developed research area. It includes IR spectra prediction, correlation of experimental results with predictions, and analysis of tunneling splittings.[52,64] An $(H_2O)_n$ cluster has $2n$ O−H stretch modes that typically fall in the 2600 to 4000 cm^{-1} range, n H−O−H bending modes between 1500 and 2000 cm^{-1}, and $6n$-6 torsional modes below 1300 cm^{-1}. Considerable care has gone into studying the factors that influence O−H stretch vibrational frequencies.[65−68] As a generalization, the frequency of an O−H* stretch mode when H* is in an H-bond is positively correlated with the length of the H-bond.[69]

The molecule H_3O^+ has three O−H stretch modes and three bending modes. The lowest bending mode (at 924 cm^{-1} by CCSD(T)/aug-cc-pVTZ [70]) has all three H's moving simultaneously toward or away from the axis of symmetry and is called the "umbrella" mode for its similarity to a folding umbrella. The OH^- molecule has one stretch and no bending modes, so an $(H_3O^+)(H_2O)_{n-2}(OH^-)$ zwitterion can be expected to have $3 + 2(n-2) + 1 = 2n$ stretch modes and $3 + (n-2) + 0 = n + 1$ bending modes. The diamonds, cube, and prism zwitterions follow this pattern, with their lowest stretch frequencies starting around 2400 cm^{-1}. Jensen[10] observed that the $H_{10}O_5$ diamond zwitterion has two exceptionally intense vibrational modes near 2700 cm^{-1} and wondered whether this could be related to an observation that the spectrum of high atmospheric water has an absorption shoulder near 2700 cm^{-1}.

7.2. Results. IR frequencies and intensities were computed by Gaussian98[20] using the harmonic approximation and were not scaled. Figure 10 is the computed spectrum for the $(H_2O)_{12}$ cluster of Figure 2d, obtained by neutralizing Figure 2a along the water wire O5−O6−O3−O2. The spectra for the other neutralized geometries are very similar and are not included.

All of the neutralized clusters follow the pattern outlined above for IR spectra of $(H_2O)_n$. The lowest stretch mode, around 2700 cm^{-1}, is for the O−H stretch in the cluster's shortest H-bond, which is the $\mathscr{B}$-to-$\mathscr{C}$ bond of the neutralization pathway (cf. Figure 9). For Figure 2d it is the O3−H63 stretch (mode 79, 2657 cm^{-1}, 2036 km/mol). The next two lowest modes, around 3100 cm^{-1}, are for the O−H stretches in the $\mathscr{A}$-to-$\mathscr{B}$ and $\mathscr{C}$-to-$\mathscr{D}$ bonds of the neutralization pathway (for Figure 2d these are O2−H32 and O6−H56).

When an H_2O in a water cluster, labeled as H_aOH_b, has both H_a and H_b donating to H-bonds, it is common but by no means universal for the O−H_a and O−H_b stretches to be coupled, producing one symmetric and one antisymmetric vibrational normal mode. Interestingly, Figure 2d has a pair of coupled stretch modes that share a common acceptor rather than a common donor. (The distinction between "coupled" and "uncoupled" requires a cutoff to be set. We define two stretches O_a-H_a and O_b-H_b to be "coupled" for modes P and Q if the ratio $M_{Pa}M_{Qb}/M_{Pb}M_{Qa}$ falls between 0.5 and 2, where M_{Pa} denotes the magnitude of the displacement of H_a for mode P, and likewise for M_{Pb}, M_{Qa}, and M_{Qb}.) Specifically, O7−H78 and O9−H98 are coupled: mode 84 (3538 cm^{-1}, 315 km/mol) is the antisymmetric stretch and mode 87 (3632 cm^{-1}, 484 km/mol) is the symmetric stretch. (Extending the customary meaning, a mode featuring a coupled stretch of O_a-H_a and O_b-H_b is "symmetric" if both bonds lengthen and contract together, and "antisymmetric" if one contracts while the other lengthens.) Coupling of O7−H78 and O9−H98 occurs in all four neutralized geometries. In the geometry neutralized via O5−O4−O1−O2, the pair of stretches O4−H54 and O2−H12, which are in the $\mathscr{A}$-to-$\mathscr{B}$ and $\mathscr{C}$-to-$\mathscr{D}$ bonds of its neutralization pathway, also meet the ratio criterion for coupling.

The computed spectrum for the zwitterion, shown as Figure 11, looks rather different from Figure 10. There are 22 O−H stretch modes above 2700 cm^{-1}, and the remaining 80 modes lie below 1900 cm^{-1}. Four of these 22 modes are of particular interest. Modes 82 (2816 cm^{-1}, 1846 km/mol) and 84 (2968 cm^{-1}, 675 km/mol) are the antisymmetric and symmetric modes respectively for coupled stretches of O5−H54 and O5−H56. These modes are noteworthy in part because O5−H5U stretching is not a major aspect of either of them. Modes 81 (2752 cm^{-1}, 1049 km/mol) and 83 (2933 cm^{-1}, 1618 km/mol) are the antisymmetric and symmetric modes respectively for coupled

stretches O1−H12 and O3−H32. Note that these two H-bonds share an acceptor, and the acceptor is the O of the OH^-.

Finding 22 stretch modes above 2700 cm^{-1} rather than the expected $2n = 24$ suggests two "missing" stretches. None of the 22 include prominent stretches of O5−H5U or O8−H82. These stretches turn up in the band normally associated with bending vibrations. Modes 77 (1809 cm^{-1}, 463 km/mol) and 80 (1874 cm^{-1}, 3382 km/mol) represent symmetric and antisymmetric coupled stretches of O5−H5U and O8−H82, respectively. Both modes also include prominent bending of O5−H54 and O5−H56. Modes 78 (1826 cm^{-1}, 1178 km/mol) and 79 (1832 cm^{-1}, 650 km/mol) represent stretches of O8−H82 coordinated with bending of all three bonds at O5 (O5−H54, O5−H56, and O5−H5U). Last, mode 66 (1372 cm^{-1}, 450 km/mol) is the umbrella mode for the embedded H_3O^+ at O5. It is the only mode lying between the highest torsional mode (1223 cm^{-1}) and the next bending mode (1650 cm^{-1}).

7.3. Discussion. The spectra of the neutralized clusters are basically consistent with those of other water clusters. They include the interesting phenomenon of a pair of acceptor-coupled stretches. To the author's knowledge this is the first time that acceptor-coupled stretches have been reported for an $(H_2O)_n$ cluster.

For the zwitterion, one has the paradox of using the harmonic approximation after declaring in section 5.3 that the harmonic approximation does a poor job of describing the PES, especially for H5U and H82. Consequently the numerical predictions based on the harmonic approximation should not be taken very seriously. Still, the calculations have provided several qualitative insights that may apply to the actual zwitterion. First, there are coupled stretches of O5−H5U−OU and O8−H82−O2 that occur well below the band normally associated with O−H stretches in water. (Stretches below 2000 cm^{-1} are well known to occur for short strong H-bonds in some organic molecules[67] and have been predicted for $H_5O_2^+$.[34−35]) Second, the zwitterion's antisymmetric stretch mode for O5−H5U and O8−H82 is the most intense mode in any of the neutralized or zwitterion spectra we calculated, with 1.5 times the intensity of the next most intense mode seen. This is due in part to the fact that it involves coordinated movement of charges that are far apart on the cluster. Recall that the intensity of a dipole oscillation varies as the square of the distance between the charges.[71] Third, the H_3O^+ of the zwitterion has an umbrella mode, which may fall in a region of the spectrum that does not have other peaks near it.

Overall, the spectrum of the zwitterion can be expected to have some very different peaks than the spectra of the neutralized geometries. In an experimental system containing an equilibrium mixture of cage zwitterions and neutralized cage clusters, some of the IR peaks from the zwitterions and from the neutralized $(H_2O)_{12}$ clusters should be distinguishable.

8. Conclusions

(1) Based on several benchmark comparisons with MP2/aug-cc-pVTZ, the method B3LYP/6-311++G** does a very good job of predicting electronic energy differences for pairs of stationary states of a water cluster when the two states are connected via transfer of one or more protons (i.e., no breaking or making of H-bonds). In particular, B3LYP/6-311++G** appears better suited for this type of problem than MP2/6-311++G**.

(2) The $H_{24}O_{12}$ cage zwitterion shown in Figure 2a is probably the smallest zwitterionic water cluster that would be stable if formed in a low temperature experimental system. It is best described as an $H_5O_2^+$ and an $H_3O_2^-$ kept apart by eight intervening H_2O molecules.

(3) Eight length three water wires connect the $H_5O_2^+$ and $H_3O_2^-$ in the cage zwitterion. (If the zwitterion is viewed as $(H_3O^+)(H_2O)_{10}(OH^-)$, then some water wires have length 4 or 5 to include transfers within the $H_5O_2^+$ and/or the $H_3O_2^-$.) Neutralization along any of these water wires leads to one of four distinct $(H_2O)_{12}$ clusters. Each neutralization reaction is endothermic at 77 K, with the range of ΔG^{neu} being 0.3 to 1.3 kcal/mol.

(4) The energetics of neutralization for the cage zwitterion support the autoionization mechanism described by Geissler et al.[62]

(5) Neutralization occurs via coordinated motion of all three water wire protons. Each pathway has a single transition state, in which the two outer protons of the wire have transferred but the middle proton has not. Activation barriers range from 2.9 to 3.8 kcal/mol at 77 K.

(6) A relaxed PES for the cage zwitterion was computed giving electronic energy as a function of the symmetrized transfer coordinates for H5U and H82, which are the bonding protons in the embedded $H_5O_2^+$ and $H_3O_2^-$. The PES has two local minima, two saddles, and a hilltop, all within 0.5 kcal/mol of each other. It shows that H5U and H82 can be expected to delocalize over a very wide area. This calls into question the validity of the harmonic approximation for the cage zwitterion and suggests that the zwitterion's ZPVE could be substantially lower than the harmonic approximation predicts.

(7) IR spectra for the zwitterion and the four neutralized geometries were computed. The neutralized geometries have a high-intensity mode near 2700 cm^{-1} corresponding to O−H stretch for the middle proton of their neutralization water wires. They also have two stretch modes near 3100 cm^{-1} for the other two water wire protons. The zwitterion has symmetric and antisymmetric modes for coordinated stretches involving O5−H5U and O8−H82. Both modes occur at very low frequencies for an O−H stretch in water (below 1900 cm^{-1}), and the antisymmetric mode has exceptionally high intensity.

(8) Study of the cage zwitterion adds to the growing list of water zwitterions that have been analyzed by ab initio methods. Patterns that are consistent between the cage zwitterion and other water zwitterions include: (a) the existence and approximate geometry of a single transition state for coordinated proton transfer along embedded water wires of length 3; (b) continuing to obey a correlation between the neutralized clusters' dipole moments, and ΔG^{neu} and ΔG^{act}; and (c) the finding of an umbrella bending mode at the H_3O^+ along with one or more high-intensity low-frequency stretch modes in the zwitterion's IR spectrum.

Acknowledgment. The author wishes to thank Joel M. Bowman for reading the manuscript and for making helpful suggestions.

References and Notes

(1) de Godoy, C. M. G.; Cukierman, S. *Biophys. J.* **2001**, *81*, 1430.
(2) Krishnamoorthy, I.; Krishnamoorthy, J. *J. Phys. Chem.* B **2001**, *105*(7), 1481.
(3) Bach, A.; Coussan, S.; Muller A.; Leutwyler, S. *J. Chem. Phys.* **2000**, *113*(20), 9032.
(4) Schweighofer, K. J.; Pohorille, A. *Biophys. J.* **2000**, *78*, 150.
(5) Sansom, M. S. P. *Curr. Opin. Struct. Biol.* **1998**, *8*, 237.
(6) Sagnella, D. E.; Laasonen, K.; Klein, M. L. *Biophys. J.* **1996**, *71*, 172.
(7) Stillinger, F. H.; David, C. W. *J. Chem. Phys.* **1980**, *73*(7), 3384.
(8) Lee, C.; Sosa, C.; Novoa, J. J. *J. Chem. Phys.* **1995**, *103*(10), 4360.

(9) Tozer, D. J.; Lee, C.; Fitzgerald, G. *J. Chem. Phys*. **1996**, *104*(14), 5555.
(10) Jensen, J. O.; Samuels, A. C.; Krishnan, P. N.; Burke, L. A. *Chem. Phys. Lett*. **1997**, *276*, 145.
(11) Plummer, P. L. M. *J. Phys. Chem*. B **1997**, *101*, 6247.
(12) Smith, A.; Vincent, M. A.; Hillier, I. H. *J. Phys. Chem*. A **1999**, *103*, 6766.
(13) Anick, D. J. *J. Mol. Struct*. **2001**, *574*, 109.
(14) Tsai, C. S.; Jordan, K. D. *J. Chem. Phys*. **1993**, *97*, 5208.
(15) Loerting, T.; Liedl, K. R.; Rode, B. M. *J. Chem. Phys.* **1998**, *108*(7), 2672.
(16) Nova, J. J.; Sosa, C. *J. Phys. Chem*. **1995**, *99*, 15837.
(17) Kim, K.; Jordan, K. D. *J. Phys. Chem*. **1994**, *98*, 10089.
(18) Xantheas, S. S. *J. Chem. Phys*. **1995**, *103*, 4505.
(19) Jaguar 3.5 and 4.0; Schrodinger, Inc. Portland, OR, 2000.
(20) Frisch, M. J.; Trucks, G. W.; Schlegel, H. B.; Scuseria, G. E.; Robb, M. A.; Cheeseman, J. R.; Zakrzewski, V. G.; Montgomery, J. A. Jr.; Stratmann, R. E.; Burant, J. C.; Dapprich, S.; Millam, J. M.; Daniels, A. D.; Kudin, K. N.; Strain, M. C.; Farkas, O.; Tomasi, J.; Barone, V.; Cossi, M.; Cammi, R.; Mennucci, B.; Pomelli, C.; Adamo, C.; Clifford, S.; Ochterski, J.; Petersson, G. A.; Ayala, P. Y.; Cui, Q.; Morokuma, K.; Malick, D. K.; Rabuck, A. D.; Raghavachari, K.; Foresman, J. B.; Cioslowski, J.; Ortiz, J. V.; Baboul, A. G.; Stefanov, B. B.; Liu, G.; Liashenko, A.; Piskorz, P.; Komaromi, I.; Gomperts, R.; Martin, R. L.; Fox, D. J.; Keith, T.; Al-Laham, M. A.; Peng, C. Y.; Nanayakkara, A.; Challacombe, M.; Gill, P. M. W.; Johnson, B.; Chen, W.; Wong, M. W.; Andres, J. L.; Gonzalez, C.; Head-Gordon, M.; Replogle, E. S.; Pople, J. A. GAUSSIAN98, Revision A.9; Gaussian, Inc.: Pittsburgh, PA, 1998.
(21) Tuckerman, M. E.; Marx, D.; Klein, M. L.; Parrinello, M. *Science* **1997**, *275*, 817.
(22) Sagnella, D. E.; Tuckerman, M. E. *J. Chem. Phys*. **1998**, *108*(5), 2073.
(23) Christie, R. A.; Jordan, K. D. *J. Phys. Chem*. A **2001**, *105*, 7551.
(24) Pavese, M.; Chawla, S.; Lu, D.; Lobaugh J.; Voth, G. A. *J. Chem. Phys*. **1997**, *107*(18), 7428.
(25) Xie, Y.; Remington, R. B.; Schaefer, H. F., III *J. Chem. Phys*. **1994**, *101*(6), 4878.
(26) Valeev, E. F.; Schaefer, H. F. *J. Chem. Phys*. **1998**, *108*(17), 7197.
(27) Auer, A. A.; Helgaker, T.; Klopper, W. *Phys. Chem. Chem. Phys*. **2000**, *2*(10), 2235.
(28) Cruzan, J. D.; Braly, L. B.; Liu, K.; Brown, M. G.; Loeser J. G.; Saykally, R. J. *Science* **1996**, *271*, 59.
(29) Estrin, D. A.; Paglieri, L.; Corongiu, G.; Clementi, E. *J. Phys. Chem*. **1996**, *100*, 8701.
(30) Gregory, J. K.; Clary, D. C. *J. Chem. Phys*. **1996**, *105*(16), 6626.
(31) Stephens, P. J.; Devlin, F. J.; Chablowski, C. F.; Frisch, M. J. *J. Phys. Chem*. **1994**, *98*, 11623.
(32) Merrill, G. N.; Gronert, S.; Kass, S. R. *J. Phys. Chem*. A **1997**, *107*, 208.
(33) Kowal, M.; Roszak, S.; Leszczynski, J. *J. Chem. Phys*. **2001**, *114*(19), 8251.
(34) Vener, M. V.; Kuhn, O.; Sauer, J. *J. Chem. Phys*. **2001**, *114*(1), 240.
(35) Vener, M. V.; Sauer, J. *Chem. Phys. Lett*. **1999**, *312*, 591.
(36) Muguet, F. F. *Int. J. Chem*. **1999**, *2*(25), 1.
(37) Testa, A. C. *Spectrosc. Lett*. **1999**, *32*(5), 819.
(38) Sadhukhan, S.; Munoz, D.; Adamo, C.; Scuseria, G. E. *Chem. Phys. Lett*. **1999**, *306*, 83.
(39) Ojamae, L.; Shavitt, I.; Singer, S. J. *J. Chem. Phys*. **1998**, *109*(13), 5547.
(40) Lee, S. H. *Bull. Korean Chem. Soc*. **2002**, *23*, 107.
(41) Vuilleumier, R.; Borgis, D. *J. Mol. Struct*. **2000**, *552*, 117.
(42) Vener, M. V.; Rostov, I. V.; Soudackov, A. V.; Basilevsky, M. V. *Chem. Phys*. **2000**, *254*, 249.
(43) Vuilleumier, R.; Borgis, D. *Isr. J. Chem*. **1999**, *39*, 457.
(44) Schmitt, U. W.; Voth, G. A. *Isr. J. Chem.* **1999**, *39*, 483.
(45) Agmon, N. *Isr. J. Chem*. **1999**, *39*, 493.
(46) Marx, D.; Tuckerman, M. E.; Hutter, J.; Parrinello, M. *Nature* **1999**, *397*, 601.
(47) Chang, H. C.; Jiang, J. C.; Chang, H. C.; Wang, Y. S.; Lin, S. H.; Lee, Y. T. *J. Chin. Chem. Soc*. **1999**, *46*(3), 427.
(48) Frey, P. A.; Cleland, W. W. *Bioorganic Chem*. **1998**, *26*(4), 175.
(49) Adams, H.; Clunas, S.; Fenton, D. E. *Chem. Commun*. **2002**, *5*, 418.
(50) Goodson, P. A.; Glerup, J.; Hodgson, D. J.; Jensen, N. B.; Michelsen, K. *J. Chem. Soc., Dalton Trans.* **2001**, *19*, 2783.
(51) Deyerl, H. J.; Luong, A. K.; Clements, T. G. Continetti, R. E. *Faraday Discuss*. **2000**, *115*, 147.
(52) Keutsch, F. N.; Saykally, R. J. *Proc. Nat. Acad. Sci. U.S.A.* **2001**, *98*(19), 10533.
(53) Clary, D. C.; Benoit, D. M.; van Mourik, T. *Acc. Chem. Res*. **2000**, *33*(7), 441.
(54) McQuarrie, D. A.; Simon, J. D. *Physical Chemistry: A Molecular Approach*, University Science Books: Sausalito, CA, 1997; p 1160.
(55) Agmon, N. *Chem. Phys. Lett*. **1995**, *244*, 456.
(56) Sagnella, D. E.; Laasonen, K.; Klein, M. L. *Biophys. J*. **1996**, *71*, 1172.
(57) Pomes, R.; Roux, B. *Chem. Phys. Lett*. **1995**, *234*, 2519.
(58) Mei, H. S.; Tuckerman, M. E.; Sagnella, D. E.; Klein, M. L. *J. Phys. Chem. B* **1998**, *102*, 10446.
(59) Sadeghi, R. R.; Cheng, H.-P. *J. Chem. Phys*. **1999**, *111*(5), 2086.
(60) Zahn, D.; Brickmann, J. *Isr. J. Chem*. **1999**, *39*, 469.
(61) Vuilleumier, R.; Borgis, D. *J. Chem. Phys*. **1999**, *111*(9), 4251.
(62) Geissler, P. G.; Dellago, C.; Chandler, D.; Hutter, J.; Parrinello, M. *Science* **2001**, *291*, 2121.
(63) Pedulla, J. M.; Jordan, K. D. *Chem. Phys*. **1998**, *239*, 593.
(64) Rodriguez, J.; Laria, D.; Marceca, E. J.; Estrin, D. A. *J. Chem. Phys*. **1999**, *110*(18), 9039.
(65) Kim, J.; Majumdar, D.; Lee, H. M.; Kim, K. S. *J. Chem. Phys*. **1999**, *110*(18), 9128.
(66) Kim, J.; Lee, J. Y.; Lee, S.; Mhin, B. J.; Kim, K. S. *J. Chem. Phys.* **1995**, *102*, 310.
(67) Kim, J.; Kim, K. S. *J. Chem. Phys*. **1998**, *109*(14), 5886.
(68) Xantheas, S. S.; Dunning, T. *Advances in Molecular Vibrations and Colloid Dynamics: Molecular Clusters*, Vol III; Bowman, J. M., Bacic, Z., Eds.; JAI: Stamford CT, 1998; pp 281−307.
(69) Jeffrey, G. A. *Introduction to Hydrogen Bonding*; Oxford University Press: New York, 1997; chapter 11.
(70) Huang, X.; Carter, S.; Bowman, J. M. *J. Phys. Chem. B* **2002**, *106*, 8182.
(71) Bernath, P. F. *Spectra of Atoms and Molecules*; Oxford University Press: New York, 1995.